AWARD NUMBER: W81XWH-14-1-0473

TITLE: **Genomic Diversity and the Microenvironment as Drivers of Progression in DCIS**

PRINCIPAL INVESTIGATOR: EUN-SIL HWANG

CONTRACTING ORGANIZATION: DUKE UNIVERSITY, Durham, NC

REPORT DATE: **October 2020**

TYPE OF REPORT: Annual Report

PREPARED FOR: U.S. Army Medical Research and Materiel Command
Fort Detrick, Maryland 21702-5012

DISTRIBUTION STATEMENT: Approved for Public Release;
Distribution Unlimited

1. REPORT DOCUMENTATION PAGE

Form Approved
OMB No. 0704-0188

1. REPORT DATE	2. REPORT TYPE	3. DATES COVERED
October **2020**	Annual Report	30Sep2019-29Sep2020

4. TITLE AND SUBTITLE
Genomic Diversity and the Microenvironment as Drivers of Progression in DCIS

5a. CONTRACT NUMBER
W81XWH-14-1-0473

5b. GRANT NUMBER
BC132057

5c. PROGRAM ELEMENT NUMBER

6. AUTHOR(S)

E.S. Shelley Hwang

E-Mail: shelley.hwang@dm.duke.edu

5d. PROJECT NUMBER

5e. TASK NUMBER

5f. WORK UNIT NUMBER

7. PERFORMING ORGANIZATION NAME(S) AND ADDRESS(ES)

Duke University
2200 W Main St Ste 710
Durham NC 27708-4677

8. PERFORMING ORGANIZATION REPORT

9. SPONSORING / MONITORING AGENCY NAME(S) AND ADDRESS(ES)

U.S. Army Medical Research and Materiel Command
Fort Detrick, Maryland 21702-5012

10. SPONSOR/MONITOR'S ACRONYM(S)

11. SPONSOR/MONITOR'S REPORT NUMBER(S)

12. DISTRIBUTION / AVAILABILITY STATEMENT

Approved for Public Release; Distribution Unlimited

13. SUPPLEMENTARY NOTES

14. ABSTRACT The project is designed to test whether genetic and/or tumor environmental heterogeneity is a driving force in progression of breast DCIS. Our project, a collaboration between Duke and ASU, have met our 60 month milestones in all 4 aims. Primary achievements for 60 months are:

1) Completed Case and control identification of 57 Pure DCIS & 61 Synchronous DCIS (DCIS with adjacent invasion) through extensive database and searching at Duke 2) Completed deep whole exome sequencing (WES) for 100 cases from 30-160ng of DNA isolated from archival FFPE specimens, 3) Comparison of analytic methods to characterize somatic mutations from this full exome sequencing, 4) Application of sequencing data for copy number assessment 5) Completed dual immune-staining on DCIS lesions using 6 pairs and 3 single antibodies, 6) Completed Image analysis of these stains, including quantitative analysis, 7) Completed identification of upstaged DCIS cases for the radiology aim, 8) Development of image analysis methods for digital mammograms, 9) Completed the validation Aim 4, including collection of DCIS that either did not progress or progressed to DCIS or invasive cancer, 10) Completed Aim 4 WES and Whole genome sequencing for 110 validation cases from 30-160ng of DNA isolated from archival FFPE 11) Full integration of team members over the past year via frequent conferencing, face to face meetings, and constant communication. This multi-disciplinary approach allowed our group to fully implement and we reach our year 5 project goals.

15. SUBJECT TERMS
DCIS, intra-tumor heterogeneity, genetic diversity, phenotypic diversity, somatic evolution, microenvironment, mammographic biomarkers

16. SECURITY CLASSIFICATION OF:			17. LIMITATION OF ABSTRACT	18. NUMBER OF PAGES	19a. NAME OF RESPONSIBLE PERSON
a. REPORT	b. ABSTRACT	c. THIS PAGE			USAMRMC
U	U	U	UU	33	19b. TELEPHONE NUMBER *(include area code)*

TABLE OF CONTENTS

	Page
1. Introduction	1
2. Keywords	1
3. Accomplishments	1
4. Impact	24
5. Changes/Problems	25
6. Products	25
7. Participants & Other Collaborating Organizations	29

1. INTRODUCTION

Ductal carcinoma in situ (DCIS) of the breast is an increasingly common diagnosis that is related to aggressive screening patterns (mammography). This "pre-invasive" lesion may progress to invasive cancer, but does so at a relatively low frequency. Nonetheless, it is commonly treated with extensive surgery, radiation, and hormonal therapy even though most of these lesions would never progress to invasive cancer. Thus, there is a pressing clinical need to stratify the risk of DCIS tumors into those in need of intervention and those that can be safely monitored without intervention. Our project is designed to address this need by characterizing the evolvability of DCIS, detecting those that have a high likelihood of evolving to malignancy versus those that are likely to remain indolent.

2. KEYWORDS

DCIS, cancer progression, intra-tumor heterogeneity, genetic diversity, phenotypic diversity, somatic evolution, microenvironment, mammographic biomarkers

3. ACCOMPLISHMENTS

What were the major goals of the project?

Aim 1. *Determine whether genetic diversity of DCIS is greater in DCIS with adjacent invasive disease compared to DCIS without progression.* Genetic divergence of the DCIS component of tumors were measured based on exome sequencing on two separate regions of the tumor, as well as normal tissue, in patients with DCIS only or Synchronous DCIS. This allowed us to confirm the association between increased genetic diversity and higher probability of progression to malignancy. Additionally, we found differences in which genes were mutating in the two tumor types by comparing the biological pathways differentially affected by somatic mutations.

60 Month Milestones:

- Protocol preparation, IRB submission and approval: (Duke eIRB Pro00054515, initial Duke approval, 5/27/2014 and renewed annually), DOD IRB approval in place – **completed**

- Case identification and tissue block selection: Through a variety of available databases, we identified a large number of cases and controls with tissue available in the Duke Pathology archives. Each potential case and control requires extensive chart and pathology review in order to determine final eligibility and usability. For example, there is sufficient amount of the DCIS lesion (>2mm size) for isolation and DCIS is not too close to invasive cancer (it extends outside the invasive component). There must be two blocks with DCIS present that are >0.8cm apart. We identified **120** cases, with pathology review- **Completed**

- Sectioning of tissue blocks: New sections from candidate paraffin blocks are cut, one H&E was stained at the beginning and end of each set prior to pathology review. Remaining sections from candidate blocks (containing a sufficient amount of the DCIS lesion) are

used for macro-dissection and subsequent DNA extraction. Additional sections were also stored for immunohistochemical (IHC) analysis of key measures of tumor and micro-environmental heterogeneity. These slides are scanned for analytic and archival purposes. We completed both cases and controls in this manner- **Completed**.

- DNA extraction of test cases: **Completed**.

- Exome sequencing of test cases: **Completed.** We chose the Genome Center at Washington University where cutting-edge methods for producing high quality data from these FFPE specimens have been developed and refined. Over the past four years, Wash U. sequenced 30-160ng from 300 individual DNA samples derived from 100 subjects (germ line sample plus 2 DCIS containing samples). They were able to derive interpretable sequence data (minimum of 40X depth at 50% coverage) from 30-160ng of FFPE DNA with qualities summarized in Figure 1, 2, 3, 4 and 5.

Case Selection

Breast tumors were classified using the World Health Organization (WHO) criteria [23]. Following pathology review, Pure DCIS, not associated with invasion and synchronous DCIS with Invasive Ductal Carcinoma (IDC), were included in this study IDC and DCIS were graded according to the Nottingham grading system [24] or recommendations from the Consensus conference on DCIS classification [25], respectively. Each case had matched normal tissues or normal node, confirmed by pathology review, to be devoid of neoplastic cells.

Table 1: Characteristics of Aim 1/2 Study Cohort

	Pure DCIS (n=57)	Adjacent DCIS (n=61)	
Age (mean)	56.9	57.5	
Race			
White	32	42	
Black	20	15	
Other	6	4	
Tumor Size (mean, cm)	3.5	4.6	
Nodal Status			
Positive	0	27	
Negative	57	34	
Grade		*DCIS*	*Invasive*
1	1	1	11
2	24	22	27
3	30	37	22

Surgery		
Lumpectomy	24	38
Mastectomy	19	23
Estrogen Receptor		
Positive	39	42
Negative	9	19
Equivocal	0	0
Progesterone Receptor		
Positive	33	38
Negative	12	23
Equivocal	3	0
HER2 Status		
Positive	0	14
Negative	0	45

Analytic Pipeline Development for identification of somatic genetic alterations: Completed.

FFPE tumor samples has numerous advantages in cancer research, but they tend to generate artifacts when used for genomic analyses. In order to minimize this limitation, we developed and validated a new bioinformatic tool (Fig. 1) to robustly identify somatic nucleotide variants and estimate intratumor heterogeneity. We optimized this strategy using 28 pairs of sequencing technical replicates—the same DNA sample sequenced twice. We validated our results on the same DNA using targeted primers using the AmpliSeq™ technology. After optimization, the mean similarity between replicates increased 5-fold, reaching 88.3% (range 66.7-100%), with a mean of 19.9 SNVs (range 1-61) per sample (Figure 3). This new algorithm provides a crucial improvement in detecting SNVs in FFPE samples. This work enabled us to achieve the main goal of this aim (see below), and has led to the development of an open-source tool that will benefit the cancer-research community (https://github.com/adamallo/ITHE). We have recently submitted this work for publication, and is currently available as a bioRxiv pre-print.

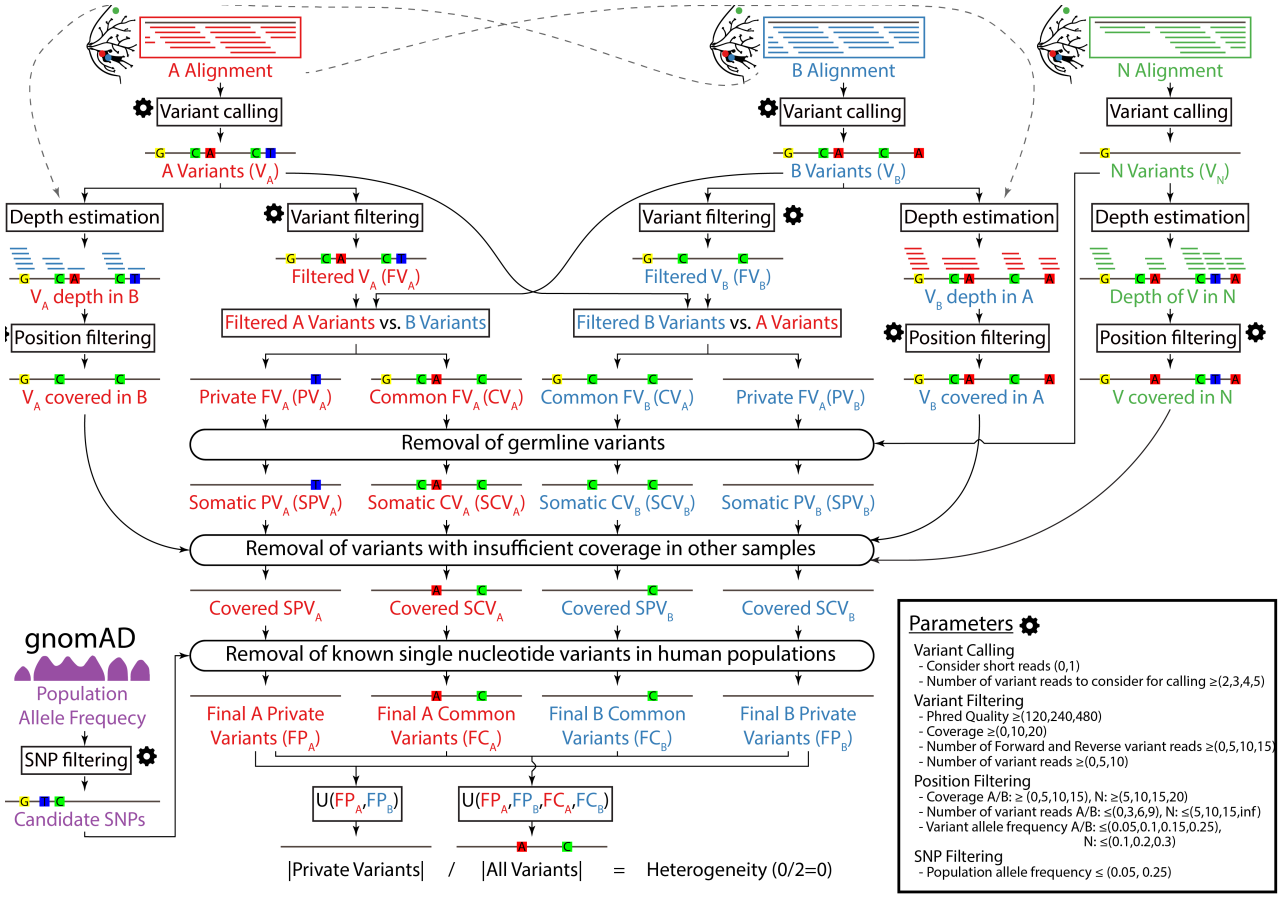

Figure 1: Flowchart of our novel algorithm to call SNV variants and estimate the genetic heterogeneity between two samples. Inputs: aligned sequences (BAM files) of the two samples (A, in red; and B, in blue) and their healthy tissue control (N, in green), population allele frequency data from the gnomAD database (single nucleotide polymorphisms, SNPs, in purple), and user-specified configuration parameters (gear icon). Outputs: estimate of the genetic heterogeneity between samples A and B, and set of variants (level of detail user-specified). The key step of this algorithm is the generation of two sets of private and common variants by comparing the variants in the two samples twice, alternatively filtering one of the sets and using all variants from the other. The parameters that control this pipeline, and the values assayed in our bioinformatic optimization, are detailed in the Parameters box.

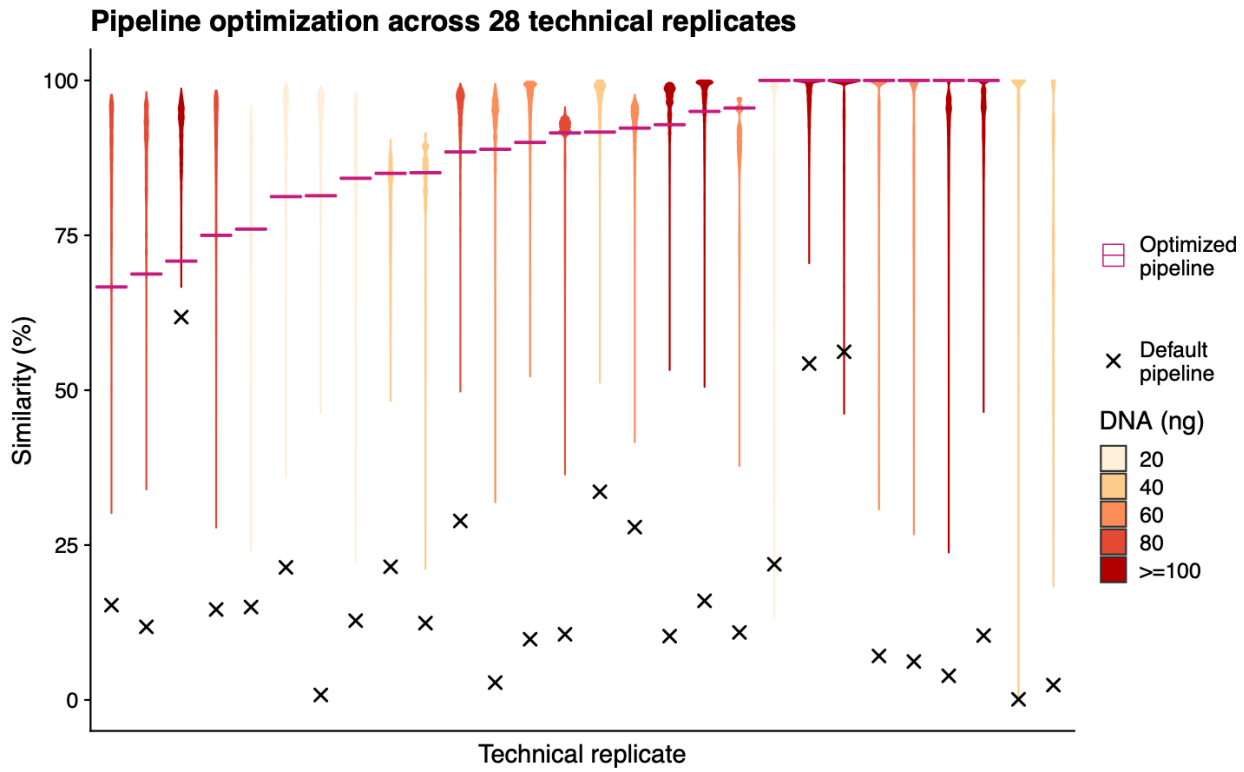

Figure 2: **Empirical optimization of the variant post-processing algorithm using technical replicates.** Each violin plot summarizes the distribution of optimization scores of the similarity obtained with 5,308,416 combinations of values of the 13 parameters that control the pipeline for one of the 28 technical replicates. (x= score before optimization; — = similarity using the optimizated parameter values for the entire data set; colors indicate the amount (ng) of DNA used as template)

Exome sequencing analysis.
Minimum coverage for inclusion in this study was 40X over at least 50% of the exome. First, reads were aligned to the reference human genome GRCh37 and variants were detected using the variant caller Platypus [26]. We annotated the variants using Annovar software [27]. Our algorithm compares two cancer samples between each other and versus the control sample. The first cancer sample analyzed with higher stringent filtering steps is compared with the second sample with low stringency and vice versa. The variants selected with the more stringent filter are retained if present also in the sample with lower stringent filter. Somatic mutations are validated on the original sequences and germ line polymorphism removed. We used the optimized pipeline to identify single nucleotide variants (SNVs), based on our 28 technical replicates and controls, as described above.

Mutational burden. There is no statistically significant difference between Pure DCIS, synchronous DCIS and IDC samples (Fig. 3). This implies that mutational burden is likely not a good biomarker for risk stratification in DCIS.

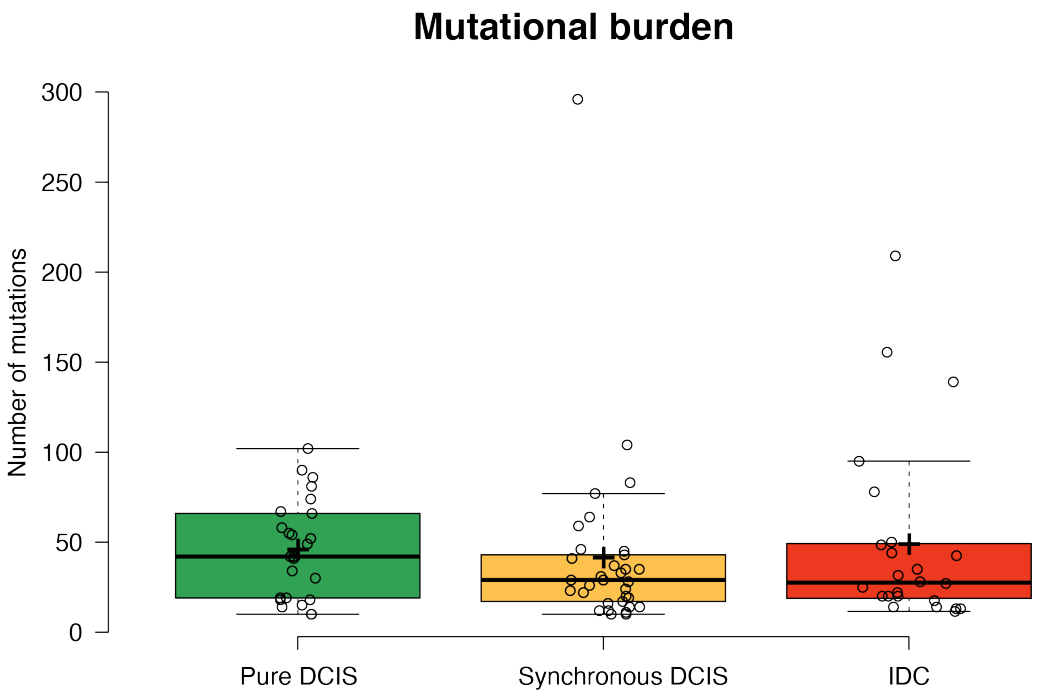

Figure 3: Mutational burden between pure and synchronous DCIS. There is no statistically significant difference between pure DCIS (n=25), synchronous DCIS (n=33), and IDC samples (n=24). Mutational burden is not diagnostic of cancer progression.

With more mutations in a tumor, we would expect that more differences would accumulate between regions. So, our null model would predict a positive correlation between mutational burden and divergence. However, there is a negative correlation between the number of mutations and the divergence in pure DCIS (Kendall's tau-b, correlation coefficient=-0.323, p=0.025), suggesting a surprising degree of genetic homogeneity in pure DCIS. In contrast, there is a positive, non-statistically significant correlation in synchronous DCIS and IDC samples themselves.

Divergence. We estimated the percent of mutations that are different between two regions of the same tumor (called genetic divergence). This can only reliably be estimated when there are sufficient mutations in the first place, to detect divergence. We limited our analysis to DCIS that had at least 10 SNVs detected by our pipeline. **We found statistically significant genetic divergence between Pure DCIS and synchronous DCIS** (adjacent to IDC) and, Pure DCIS and IDC (one-way ANOVA (F (2,75) = 8.959, p< 0.001, post-hoc Tukey test: Pure DCIS vs synchronous DCIS, p=0.005; Pure DCIS vs IDC, p<0.001, synchronous DCIS vs IDC=NS), Figure 4.

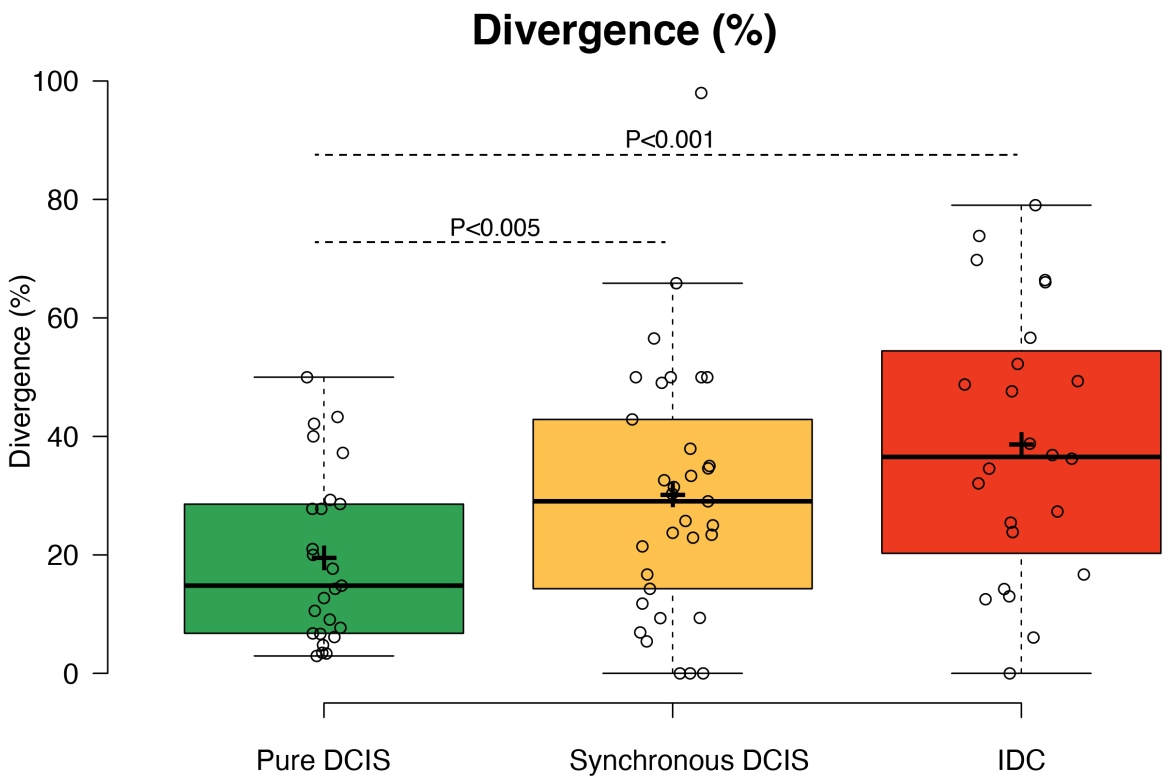

Figure 4: Genetic divergence between pure and synchronous DCIS. The genetic divergence between two regions of the same tumor is higher in synchronous DCIS and IDC samples than in Pure DCIS samples (Anova, p<0.001). Here divergence in the IDC column is calculated as the differences in the mutations carried in the one IDC sample compared to the adjacent DCIS sample.

Functional analysis. We further analyzed the mutated genes to evaluate the molecular processes or signaling pathways that are deregulated based on DAVID (https://david.ncifcrf.gov) gene functional analysis. Pure DCIS and synchronous DCIS have a distinct mutational profile. Cell adhesion genes (e.g. cadherins) are statistically significantly enriched in synchronous DCIS patients (Fold enrichment=6.11, p<0.001 FDR, DAVID). Pure DCIS patients have an enrichment of immune-related genes (Fold enrichment=11.02, p=0.047 FDR, DAVID). There is a marginal overlap between pure DCIS and synchronous DCIS mutated genes (8.6%). Functional gene analyses show a difference between pure DCIS and synchronous DCIS patients compatible with the acquired invasive capacity of synchronous DCIS cells. It is unclear why immune related genes would be more often mutated in pure DCIS than in DCIS adjacent to IDC. The enrichment of the cell adhesion genes mutated in the synchronous DCIS may predict their evolution of invasion into the surrounding tissues.

Conclusion

Our results for Aim 1 support our hypothesis that the genetic diversity (intra-tumor heterogeneity) of DCIS is associated with progression to IDC. Genetic divergence is higher in DCIS that is adjacent to IDC than in pure DCIS. This is the first time that genetic divergence

has been tested as a biomarker in DCIS. Note that just measuring the number of mutations that can be detected in the two forms of DCIS does not distinguish them. So the typical measures that cancer genomics researchers use does not provide signal of risk of progression. It is only when we quantify genetic diversity within the tumors that we begin to see significant differences. This work has also generated a widely applicable bioinformatics tool for the large community of cancer biologists who wish to sequence tumor from small amounts of FFPE material.

Our results are consistent with our (evolutionary) theoretical understanding of cancer. Genetic heterogeneity is the source of cancer's adaptive ability. Genetic variability determines the emergence of new clones capable of adapting to new microenvironments and to develop resistance to therapeutic treatments.

Aim 2. Determine whether phenotypic diversity of DCIS and the tumor microenvironment (TME) is greater in DCIS with adjacent IDC compared to DCIS without IDC. Since genomics is not the sole driver of tumor behavior, we phenotypically characterized DCIS and its microenvironment including markers of hypoxia, migration, proliferation, matrix organization, and immune signaling in the same samples used in Aim 1. We computed measures of microenvironmental heterogeneity to determine if the specific components of the TME, or the differences between TMEs from the same tumor, distinguishes between DCIS with and DCIS without adjacent IDC.

60 Month Milestones:

- IHC staining of candidate markers on all cases – **completed**
- Expert scoring of all markers on all cases – **completed**
- Data analysis using distance metrics to determine which markers demonstrate significant heterogeneity that distinguishes pure DCIS from mixed DCIS/invasive cases – **completed**
- Stain Aim 4 cases with the most promising markers of tumor and microenvironmental heterogeneity – **completed**
- Scan IHC and H&E stained slides for Automated image analysis (AIA) – **completed**
- Training and validation of AIA for the identification and enumeration of cell types (epithelial, stromal, lymphocytes, blood vessels). Computer algorithms are trained by expert identification of cell types (study pathologist, Allison Hall). Accuracy of the computer identification is evaluated by comparison back to the expert scoring. Apply methods for quantitative image analysis – **completed**
- Test computer vision methods for measuring nuclear size as a surrogate for tumor grade – **completed**

Biomarker Staining and Scoring

We have analyzed our phenotypic diversity markers on a total of 118 cases (57 pure DCIS, 61 mixed DCIS/ invasive, Table 1). To evaluate these elements, we have used a detailed expert scoring that captures the distribution of intensity of staining. This allows us to fully evaluate heterogeneity between regions of the cancer following the original study design and the genetic analyses.

Table 2: Aim 2 IHC Markers

Scoring Method	Marker	Pure (n=57)	Invasive (n=61)
	ALDH_DCIS	57	56
	ALDH_stroma	57	56
	CA9	56	58
	ER_DCIS	48	56
	FASN_DCIS	39	44
	GLUT_DCIS	56	57
	COX2	57	54
Intensity (class 1-4)	HER2_DCIS	55	56
	PFAK_DCIS	56	57
	PR_DCIS	57	55
	RANK_DCIS	57	55
	COL15	55	56
Hotspot (class 1-4)	CD31	48	50
	CD68_macrophage index	56	57
Percentage	Ki67	57	56
(Class 1-2: pos/neg)	FOXP3	51	58
	P63	54	55

For each IHC marker, the percent of cells in each staining category (Table 2) were used to define a phenotypic profile of a region. Each region also has a genetic profile generated using the two DCIS regions that were sequenced in Aim 1 (Aim 1). We calculated three types of statistics for each marker:

1. Mean intensity score = a weighted sum of the scores, weighted by staining intensity, normalized by the maximum possible staining intensity, which is a measure of the average amount of protein expression per cell, in the sample.
2. The mean Shannon entropy across the four intensity levels of staining, which is a measure of the within sample heterogeneity among cells for the protein.
3. The Earth Mover's Distance, which is a measure of between sample heterogeneity.

Mean Intensity

Figure 55a shows that only the mean of GLUT1 staining is statistically significantly different between the pure DCIS and the DCIS that is adjacent to invasive disease (unadjusted $p = 0.004$). CA9 may also help distinguish the two groups (unadjusted $p = 0.07$).

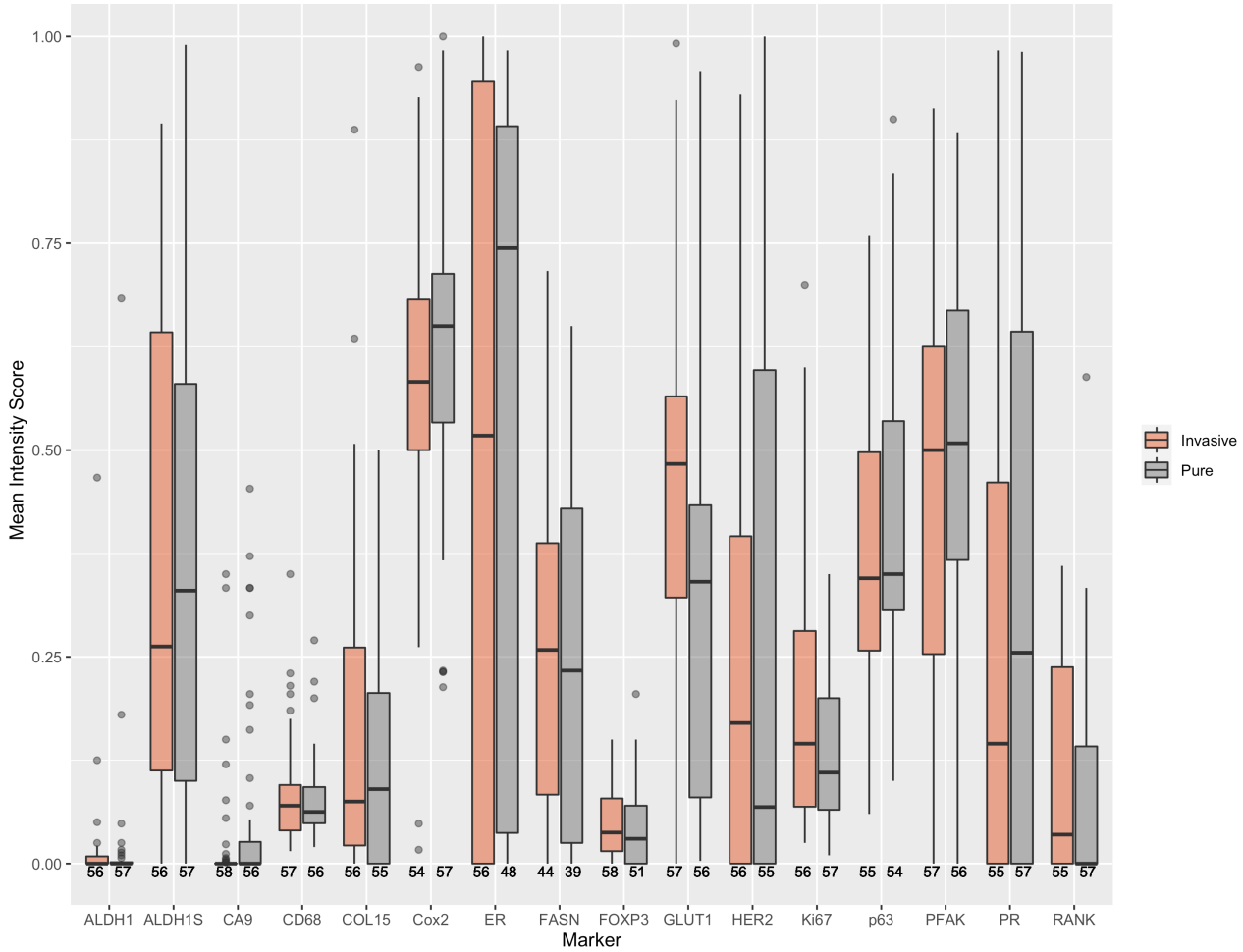

Figure 5a. Distributions of mean intensity for all Aim 2 markers. Only GLUT1 expression significantly differs between the groups, with greater expression in the DCIS adjacent to invasive cancer.

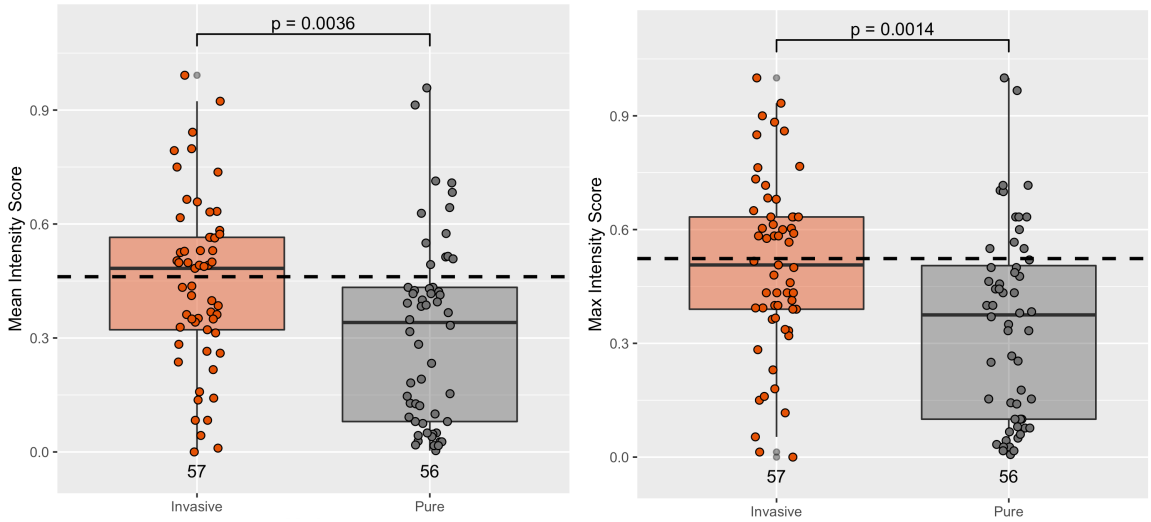

Figure 5b. Distributions of mean and maximum intensity score for GLUT1. There is significance in both these comparisons, with pure DCIS samples showing lower staining intensity. Horizontal lines represent the optimal cutoff for a logistic model classifier.

Within Sample Heterogeneity

Figure 5c shows the distributions of within sample heterogeneities as measured by the Shannon entropy statistic and averaged over the two samples from each patient. The only statistically significant difference we found was in ER staining (unadjusted $p = 0.02$), which is more homogeneous in the pure DCIS samples. Within sample heterogeneity of PFAK may also be relevant for distinguishing the groups (unadjusted $p = 0.06$).

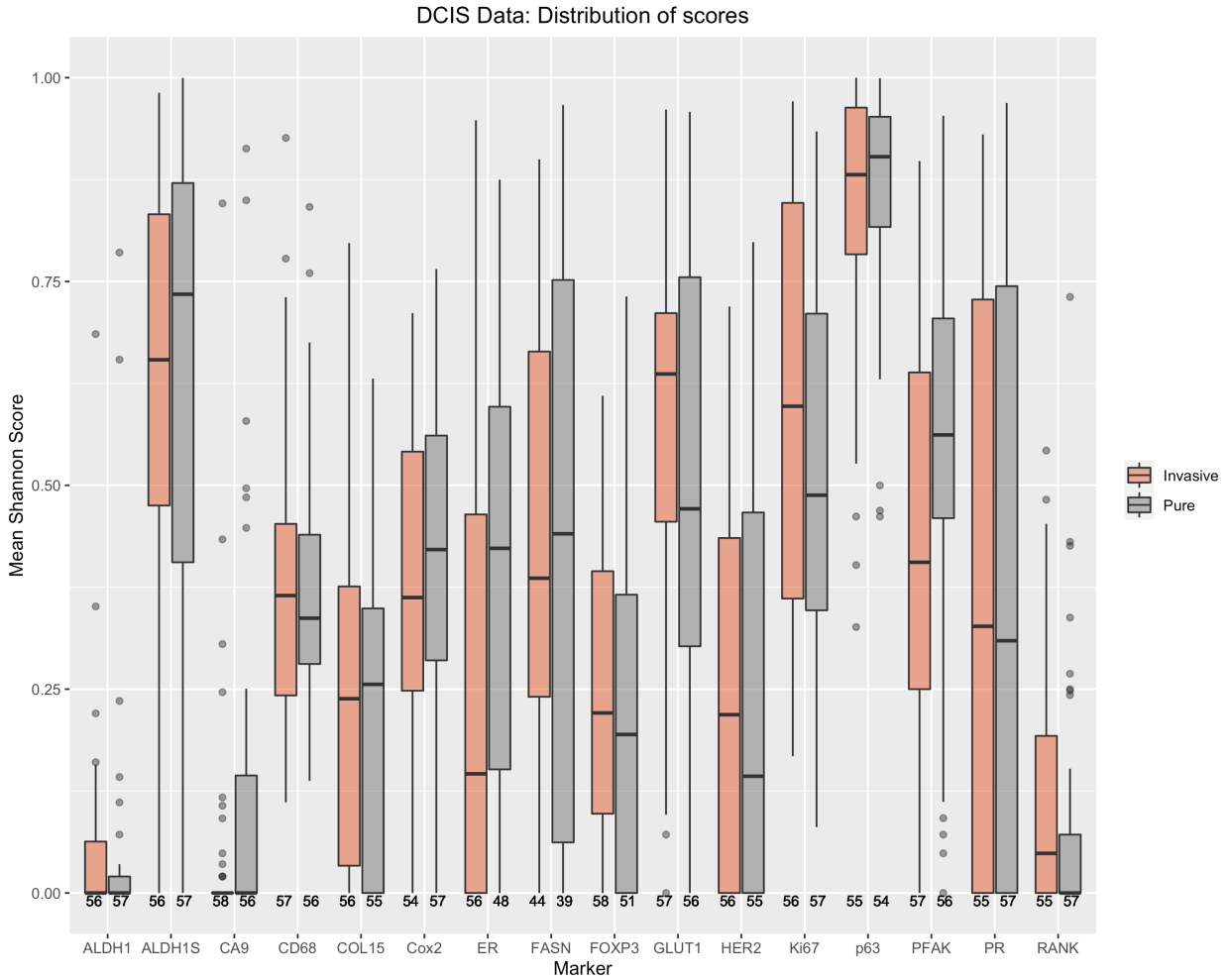

Figure 5c. Mean Shannon diversity score of marker staining's, averaged over the two samples for each patient. Only the Shannon diversity of ER is statistically significantly different between the two groups. Staining of ER is more homogeneous in the DCIS that is adjacent to invasive disease and more heterogeneous in the pure DCIS patients.

Between Sample Heterogeneity

We tested a number of measures of differences between samples. These are essentially metrics for how different are the distributions of staining intensities between the two samples from a tumor. We found that the Earth Mover's Distance was the best. This measures how much of one distribution you would have to move to transform it into the other distribution. It also takes into account how "far" you would have to move the different parts of the distribution. So the maximum Earth Mover's Distance would involve transforming a distribution of all cells not staining into a distribution of all cells staining with high intensity (or vice versa). Figure 6d shows the Earth Mover's distance between the two samples from each patient. We found a statistically significant difference in the Earth Mover's Distance between pure DCIS patients and DCIS adjacent to invasive disease for GLUT1 (unadjusted $p = 0.007$) and HER2 (unadjusted $p = 0.01$).

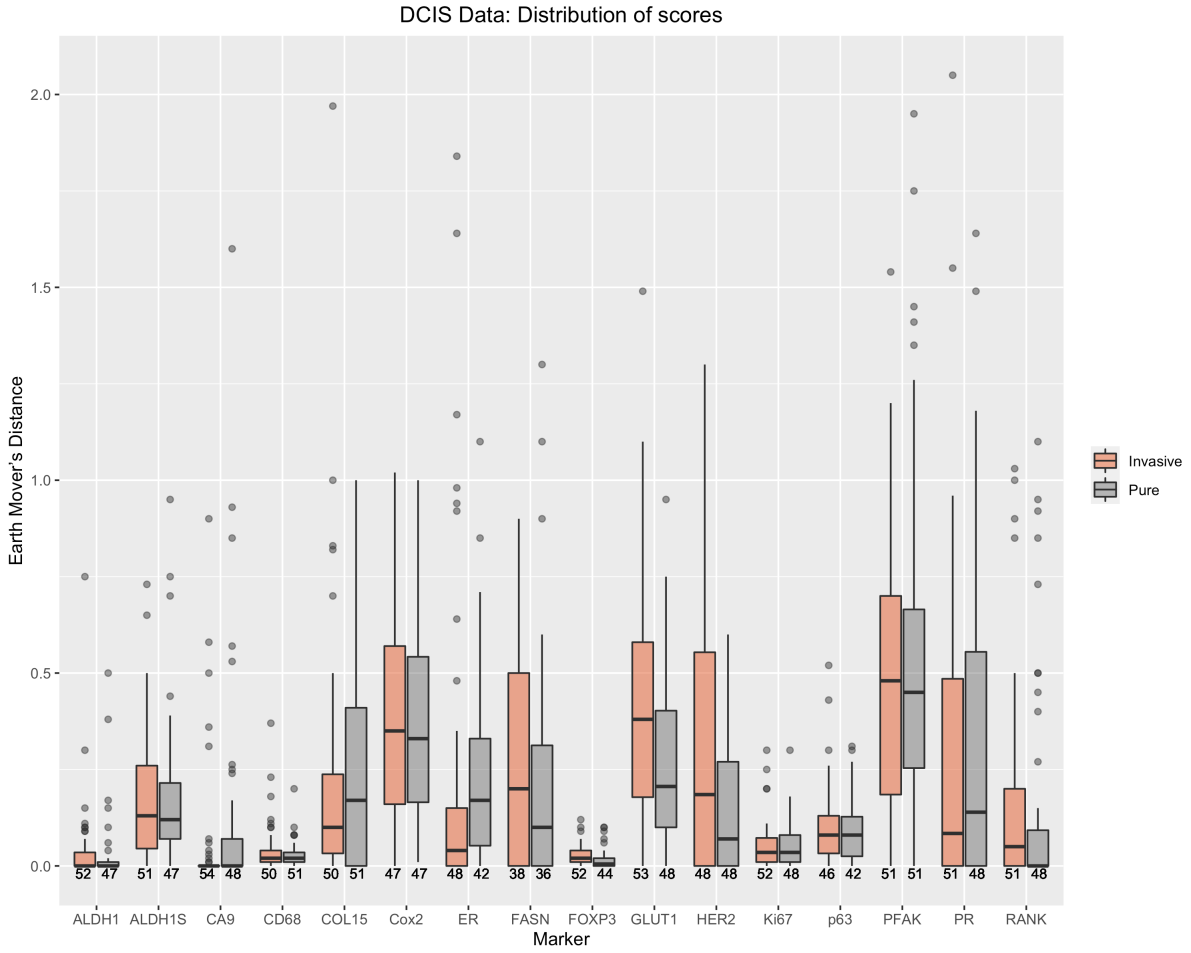

Figure 5d. Distributions of the Earth Mover's Distance for all markers and groups. This is a measure of the difference between two distributions. DCIS that is adjacent to invasive disease shows more differences between samples than pure DCIS for GLUT1 (p=***) and HER2 (p=***).

Multivariate Discrimination of Pure from Adjacent DCIS

We took the 6 variables that showed statistical significance, or near statistical significance, for distinguishing pure DCIS from DCIS that is adjacent to invasive disease, and put them together in a multivariate logistic regression to determine which measures have independent predictive value. Those variables included mean intensity scores for GLUT1 and CA9, within sample heterogeneity (Shannon) scores for ER and PFAK, and between sample heterogeneity (Earth Mover's Distance) scores for GLUT1 and HER2. When combined, only within sample heterogeneity of ER (unadjusted p = 0.002) and between sample heterogeneity of GLUT1 (unadjusted p = 0.008) remain statistically significant. This two variable model has an area under the curve (AUC) of 0.72 for the receiver-operator characteristic (ROC) curve for distinguishing pure DCIS from DCIS adjacent to invasive disease. When we added genomic divergence from Aim 1 to the model, our sample size (and statistical power) shrinks to 55 patients, because we can only reliably measure divergence in tumors with at least 10 mutations. In this case, all three measures provide independent predictive value: Within sample heterogeneity of ER (unadjusted p = 0.004), between sample heterogeneity of GLUT1 (unadjusted p = 0.02), and divergence (unadjusted p = 0.02). That three variable linear model provides an AUC=0.85 for the ROC curve. None of these p-values remain significant after the most conservative Bonferroni multiple testing adjustment, but these

analyses were applied to our training/discovery cohorts (Aims 1&2). We will deal with the potential of false positives in this analysis by testing just GLUT1 (between sample heterogeneity), ER (within sample heterogeneity) and genomic divergence in our validation cohort (Aim 4).

Tumor Infiltrating Lymphocytes (TIL)

Typically, cancer researchers measure the absolute number of lymphocytes that infiltrate a tumor. However, the exact spatial relationships between lymphocytes and neoplastic cells may indicate important biological interactions between those cells. The Yuan lab has developed deep neural network methods to automatically identify ducts and classify epithelial, lymphocyte and stromal cells in H&E images. This allows us to calculate spatial statistics of the relationships between those cell types in DCIS ducts. We found that in the DCIS that is adjacent to invasive disease, lymphocytes colocalized with DCIS cells more than in the pure DCIS cases (Figure 5e), even though there were fewer lymphocytes infiltrating those ducts (Figure 5f). These results have been accepted for publication in NPJ Breast Cancer [3].

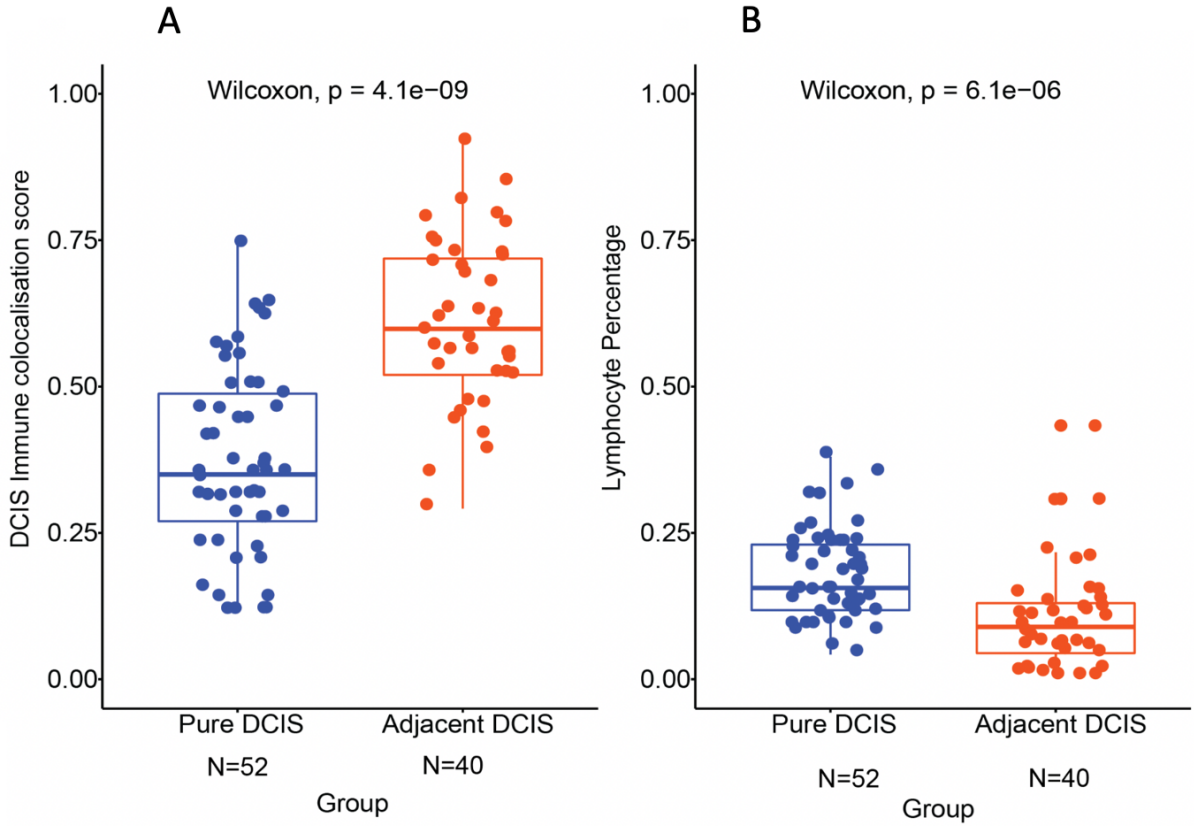

Figure 5e. Comparison of lymphocyte count (A) and colocalization (B) in pure and synchronous DCIS. If we only quantify the total number of lymphocytes that have infiltrated the DCIS ducts, we find that there are fewer infiltrating lymphocytes in DCIS that is adjacent to invasive disease ($p < 10^{-5}$), however they tend to be more spatially closely associated with the DCIS cells than in the pure DCIS cases. Using the Morisita-Horn index for measuring the intermixing or colocalization of DCIS cells and lymphocytes, we found that there is more colocalization of those cell types in DCIS that is adjacent to invasive disease than in pure DCIS ($p < 10^{-8}$).

Digital Pathology Spatial Analysis of DCIS Microenvironment.

To enable spatial mapping of hypoxia and T cell regulation in DCIS, we designed an end-to-end deep learning framework for histology image analysis. We hypothesise, and provide preliminary data, that T-reg recruitment is spatially dependent on hypoxic microenvironment and these two spatial factors underpinned evolution of DCIS to invasive cancers. There are 120 pairs of dual markers, full face section IHC CA9-FOXP3, from 59 patients with pure DCIS, 61 DCIS adjacent to invasive. Our primary aims were: 1) to develop and validate a computational pipeline that accurately classify cells based on hypoxic status and T-regulatory cell marker; 2) to test spatial dependency of T-cell regulation on hypoxia; 3) to compute microenvironmental divergence to determine if specific components of the TME, or the divergence between TMEs from the same tumour, differs between DCIS with and DCIS without adjacent IDC.

Spatial heterogeneity of hypoxia in DCIS was evident in some tumours (Figure 6a). To objectively and accurately score hypoxia (CA9) and its spatial relationship with Foxp3-expressing lymphocytes within DCIS samples, we developed a deep learning approach using convolutional neural networks (CNNs, Figure 6b). To train deep learning models, 35883 single cell annotations were collected from collaborating pathologists in 12 whole section tumour images with double staining of CA9 and FOXP3. Three deep learning methods were tested and their performance on the test set was compared. SCCNN achieved the highest, 88.6% accuracy for cell classification in the validation set.

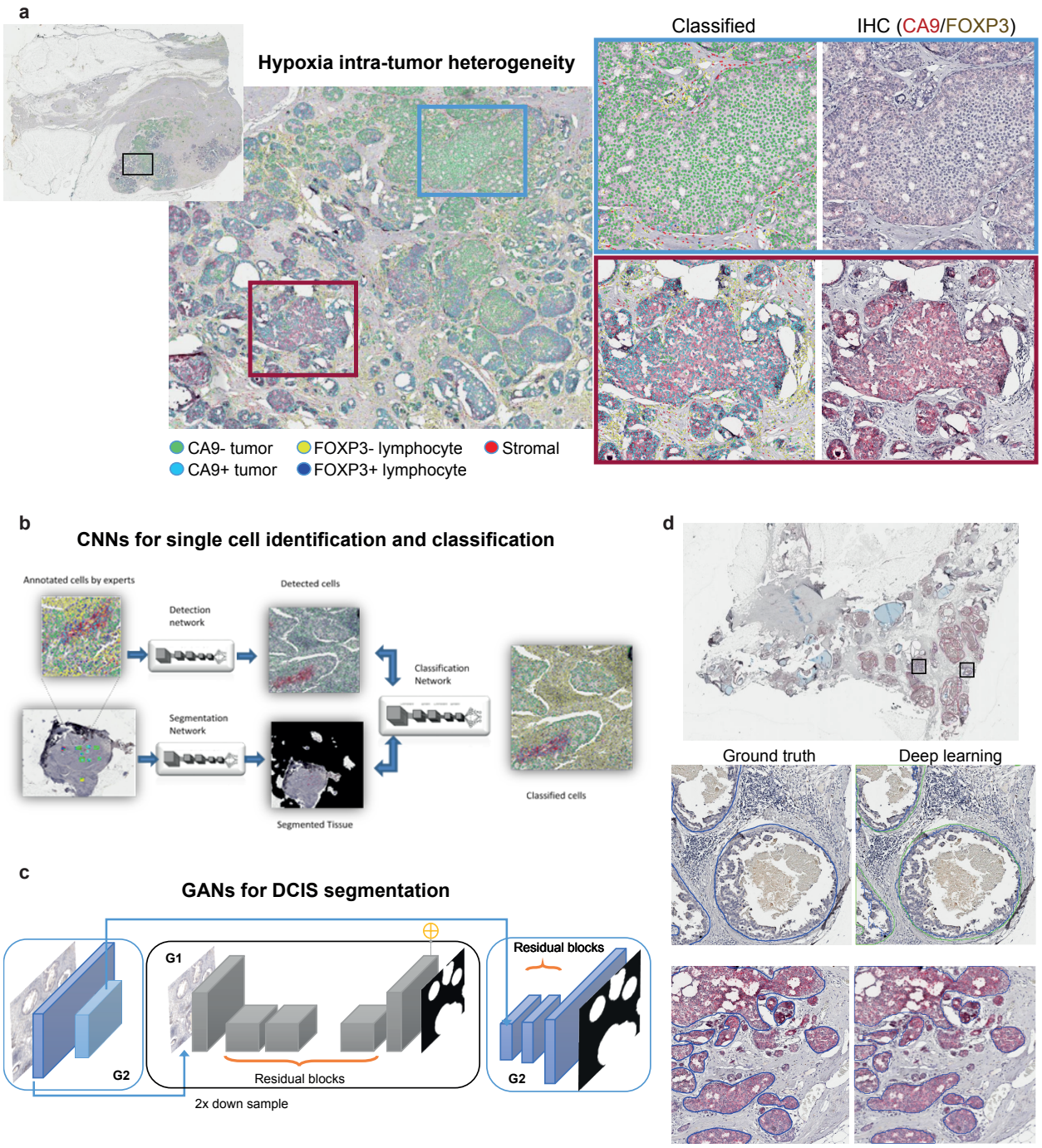

Figure 6. Studying intra-tumor heterogeneity of hypoxia in DCIS using deep learning and digital pathology. a. An illustrative example of a DCIS tumor with high spatial intra-tumor heterogeneity of hypoxia. Shown are images of IHC dual-staining with CA9 and FOXP3, cells were classified into 5 types based on their expression of CA9 and FOXP3 and morphological features. b. The deep learning pipeline using Convolutional Neural Networks (CNNs) for single-cell analysis. c. Generative adversarial networks (GANs) for semantic segmentation of individual DCIS ducts. d. An example of DICS tumor where individual DCIS ducts have been segmented using GANs. Two high resolution examples show ground truth obtained from annotations by pathologists and output from GANs.

We employed generative adversarial networks (GANs) for the detection and segmentation of DCIS ducts in CA9/FOXP3 IHC images (Figure 6c-d). Given the large size of whole slide images, we used an extended version of GANs (HD-GAN) for analyzing high-resolution histology images and generating semantic label maps corresponding to the target regions on the whole slide images. This method is based on conditional GANs that uses a robust adversarial learning objective together with new multi-scale generator and discriminator architectures. This model has enabled us to analyze our images at high image resolutions (i.e. 2048×2048 resolution) and predict large and variable size and shape objects on the whole slide images (Supplementary Figure 1). The network was trained on 18 whole slide images and the performance of the model was tested on 8 unseen slides. HD-GAN achieved average Dice score of 0.89 for the segmentation performance, and the accuracy of 0.88 for detection performance. This model outperformed other approaches tested owing to the inclusion of paired image supervision and wider field of view that was considered for preparing the training and the testing datasets.

These AI developments enabled us to quantify the spatial relationship between T cell regulation and hypoxia in DCIS. Our preliminary results in a subset of these samples showed no significant difference in the abundance of CA9 or FOXP3 cells between pure and adjacent DCIS groups. However, increased spatial colocalization of CA9+ tumor and FOXP3+ lymphocytes, quantified using the Morisita-Horn index, was observed in adjacent samples. We are in the process of confirming this observation in the remaining samples.

Aim 3. *Create and test a computational learning algorithm to compare mammographic characteristics and diversity measures in pure DCIS compared to DCIS with IDC.* A weighted computational algorithm using mammographic features of lesional and stromal characteristics as well as heterogeneity measures derived from Aims 1 and 2 will be constructed. The tool will be designed to allow for radiologic discrimination between good and poor prognosis DCIS, and will be evaluated in a validation set.

60 Month Milestones:

- Collection of 700 Duke DCIS mammography cases – completed.
- Development of mammography radiomics model on 400 cases to predict upstaging – **completed.**
- Testing of mammography radiomics model to predict upstaging on 300 independent cases – **completed.**
- First stage of radiologist observer study to predict upstaging from mammography – completed.
- Second stage of radiologist observer study to predict upstaging from mammography – **completed.**
- Detection of microcalcification clusters in mammography using anomaly detection approach – **completed.**

We performed three major studies this year: (1) prediction of upstaging using radiomics features from mammography synthesized by a machine learning model, (2) two-stage radiologist observer study to improve their performance in predicting upstaging from mammography, and (3) detection of breast microcalcifications using an unsupervised deep learning approach for anomaly detection. Each study is described below.

First, we concluded our study to predict upstaging to invasive cancer using mammography. The manuscript has been submitted to the Journal of Clinical Oncology. This large cohort of 700 Duke Health subjects is the largest DCIS mammography dataset to date. Note that all our previous studies were all based on a much smaller subset of 137 cases. The 700 cases included 114 cases (16.3%) that were upstaged, and were split randomly into 400 cases for training and 300 for testing. Logistic regression with regularization was used as the machine learning classifier, with or without stabilized feature selection. 109 radiomic features describing individual microcalcifications and microcalcification clusters were digitally extracted. In addition, four clinical features were extracted from core biopsy pathology reports. Four models were evaluating in the training set, and the model with the highest performance was identified. For the test set, the best model using all radiomic and clinical features predicted upstaging with receiver operating characteristic (ROC) area under the curve (AUC) of 0.695 (95% confidence interval [CI]: 0.607-0.782).

As shown below in Figure 8, for hypothetical clinical situations requiring high sensitivity, the best model can provide 90% sensitivity, 25% specificity, and odds ratio of 3.03. For alternative scenarios requiring high specificity, the model can provide 90% specificity, 31% sensitivity, and odds ratio of 4.10.

In conclusion, machine learning models using radiomic features from standard mammography can predict DCIS upstaging. Such predictive models can refine clinical decision making and treatment planning.

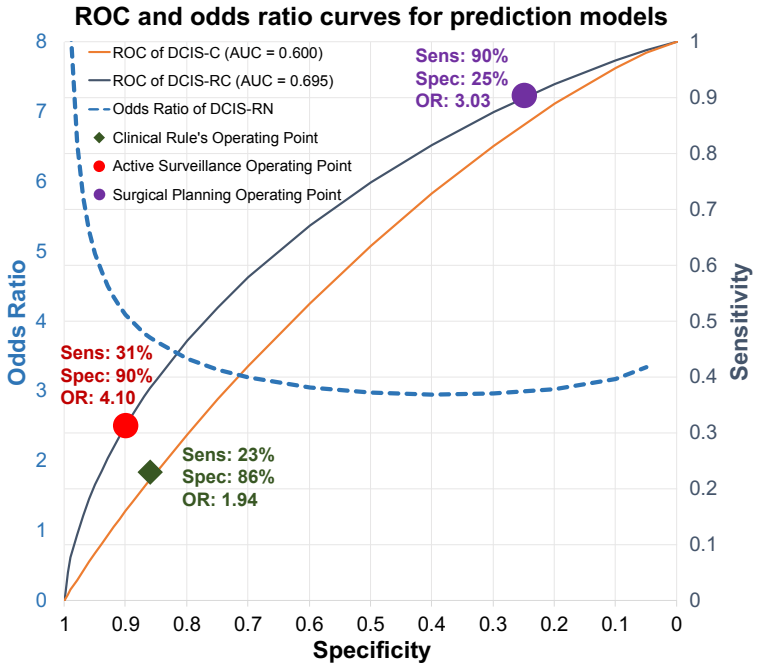

Figure 7 ROC and Odds Ratio Curves of Prediction Models**.** ROC curves are shown for two models: DCIS-RC (gray) and DCIS-C (orange). Both ROC curves are plotted as sensitivity (secondary vertical axis on the right) vs. specificity (horizontal axis). Blue dashed line is odds ratio curve, plotted as odds ratio (primary vertical axis on left) vs. specificity (horizontal axis). Three operating points are shown with symbols and are described in text: current clinical trials for active surveillance (green diamond), high-sensitivity active surveillance (purple circle); high-specificity surgical planning for sentinel node biopsy alongside with lesion removal surgery (red circle).

Second, we concluded our two-stage observer study to improve radiologists' ability to predict upstaging of DCIS to invasive disease on mammography. The second stage study was submitted and published this year in *AJR American Journal of Roentgenology* [8]

For the first stage of the observer study, nine radiologists reviewed the mammograms in the first cohort of 150 cases in a blinded fashion and scored the probability of upstaging to invasive disease. The radiologists then reviewed the cases and results collectively in a focus group to develop consensus criteria that could improve their performance. Using those new diagnostic criteria, the radiologists then reviewed the second cohort in the same, blinded fashion.

In the first round, mean reader performance was AUC of 0.623. In the focus group, radiologists agreed that 1) an associated mass, asymmetry, or architectural distortion, 2) larger extent of calcifications if densely packed, and 3) focusing on the most suspicious rather than most common features, better predicted upstaging. There was agreement that BI-RADS descriptors do not adequately characterize risk of invasion and that microinvasive disease and smaller areas of DCIS will have poor prediction estimates. The mean reader performance significantly improved in the second round (mean AUC: 0.765; AUC range: 0.617-0.852; p=0.045).

In conclusion, a mixed-methods two-stage observer study identified factors that helped radiologist significantly improve their ability to predict upstaging of DCIS to invasive disease.

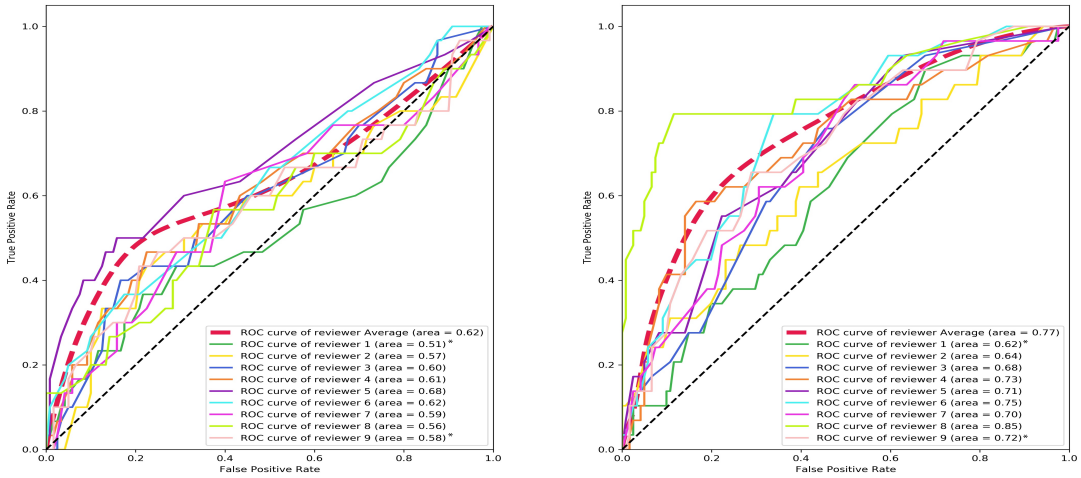

Figure 8. Reader performance in rounds 1 (left) and 2 (right) plotted as ROC curves demonstrating significant improved performance using the new diagnostic criteria developed in this study. Mean AUC (red dash) increased from 0.623 to 0.765 (p=0.045).

Third and finally, we conducted an additional study using deep learning to perform unsupervised anomaly detection for microcalcification clusters in mammography. This study was submitted to the *IEEE Transactions in Medical Imaging* and is now under revision. Addressing a fundamental challenge of sparsity of positive cases, we proposed to detect microcalcifications using an unsupervised, one-class, deep convolutional autoencoder. By training autoencoders with a large number of over 50,613 mammograms from 10,944 negative subjects, we showed that the model will encode features extracted from these images rather than malignant microcalcifications that it has never seen. Lesion detection was achieved by analyzing the residual map from structural similarity index to take into account subtle differences among microcalcifications and the neighboring background. Our pixel-wised individual microcalcifications' detection achieved an AUC of 0.98 on a validation set. Further evaluation of microcalcification clusters' detection at the image level achieved a sensitivity of 66% at 1.0 false positive per image on testing data.

Examples of segmented cluster is shown in Fig. 9, where different thresholds were applied to the residual map to yield different segmentations of clusters. The resulting free-response ROC or FROC curve is shown in Fig. 10. The model achieved a sensitivity of 66% at 1.0 FP per image, and 75% at 3.1FP per image.

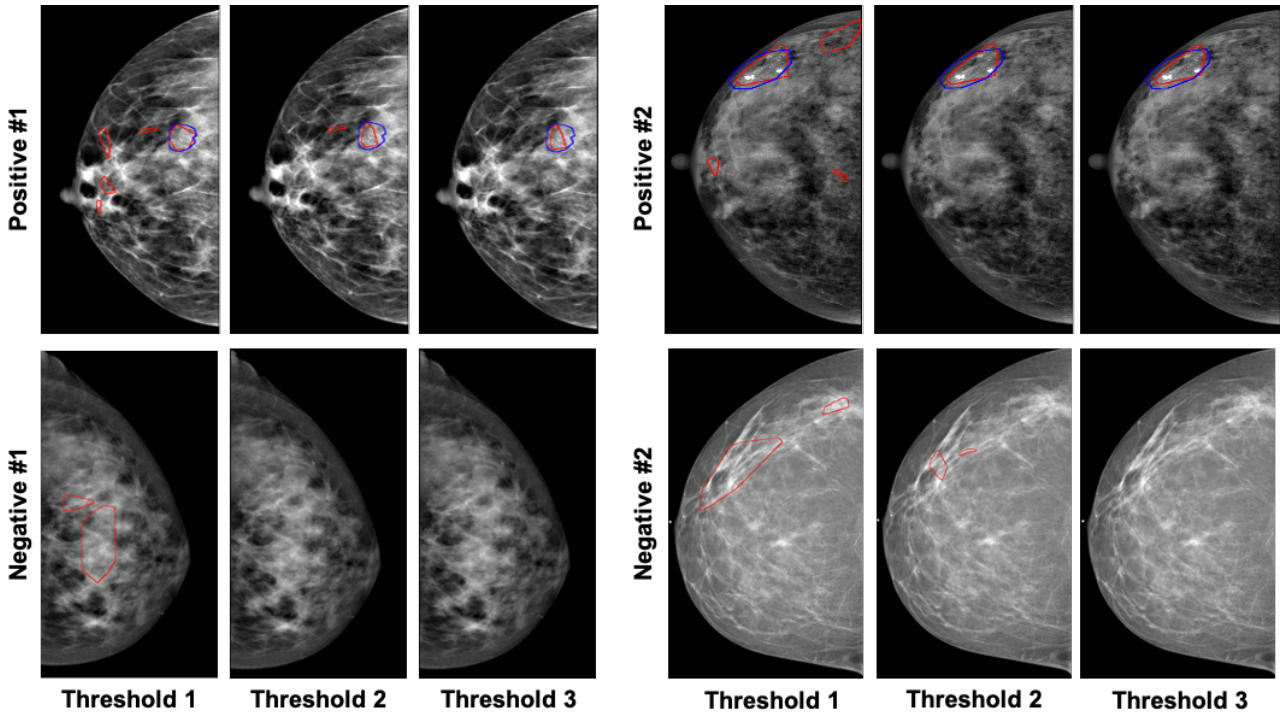

Figure. 9. Examples of post-clustering method. Blue polygons represent radiologists masked lesions, while red polygons represent our algorithm detected MC clusters. Three thresholds are selected at 3 false positive per image, 1 false positive per image and 0.5 false positive per image, respectively.

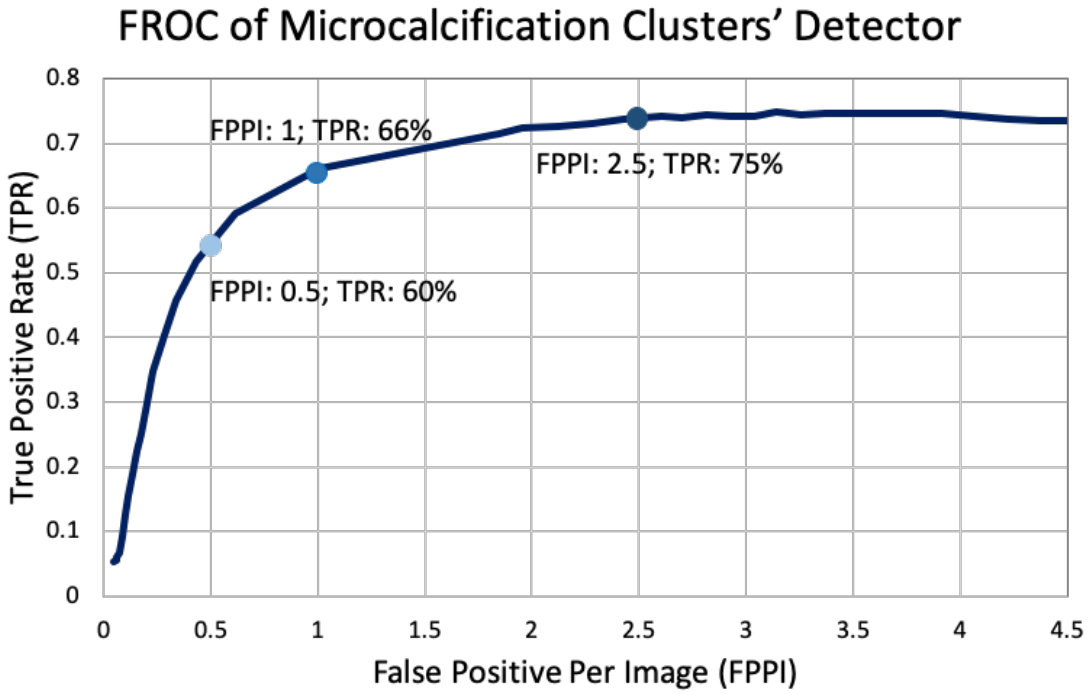

Figure. 10. Free-response ROC (FROC) of Microcalcification Cluster Detection. Performance of the model is shown as sensitivity (true-positive rate or TPR) as a function of the specificity (false positives per image for FPPI). Several operating points demonstrate the tradeoff between these two metrics.

Aim 4. *Test the predictive performance of the best diversity measures in an independent validation set of pure DCIS with and without subsequent invasive recurrence.* Genotypic and phenotypic measures of diversity derived from Aims 1-2 will be applied to an independent case-control, longitudinal, tissue bank of DCIS with and without invasive or DCIS recurrence to validate their utility. The Duke IRB approved protocol was approved at 12 sites. In the last two years, we accrued cases of pure DCIS with no disease recurrence or cases that recurred with DCIS or invasive cancer. Slides were shipped to Duke for macro-dissection followed by DNA analysis and immunodetection of phenotypic heterogeneity.

60 Month Milestones:

- We obtained approval to obtain specimens through the Translational Breast Cancer Research Consortium (TBCRC) and Duke IRB approval. We identified 12 high volume academic medical center consortium members who obtained regulatory approval, DOD approval and MTA's- – **completed.**

- The REDCap database is used for data entry online and slide inventory control. To date we have obtained cases from all 12 sites. We received 106 cohort 0, 75 cohort 1 and 61 cohort 2 cases thus achieving final project accrual and analysis goals – **completed.**

- Aim 4 WES data analysis is near completion and data is in preparation for a manuscript– **in process.**

- Nanostring was completed on a subset (n=20) of these cases. Additional Nanostring cases are currently under way **– in process.**

Table 3: Aim 4 Clinical summary Table

	Pure DCIS (N=106)	DCIS with DCIS recurrence (N=75)	DCIS with Invasive recurrence (N=61)
Year of Diagnosis			
Median	2009	2008	2006
Age at Diagnosis			
Median	54.7	57	50.6
Mean (±SD)	55.5 (± 9.3)	55.8 (± 9.6)	52.9 (±9.6)
Grade			
1	6 [5.7%]	7 [9.3%]	5 [8.2%]
2	38 [35.8%]	33 [44.0%]	20 [32.8%]
3	62 [58.5%]	35 [46.7%]	36 [59.0%]
Treatment			
Lumpectomy w Radiation	61 [57.6%]	45 [60.0%]	28 [46.0%]
Lumpectomy no Radiation	5 [4.7%]	20 [26.7%]	13 [21.3%]

Lumpectomy Radiation	1 [0.9%]	1 [1.3%]	1 [1.6%]
Unknown			
Mastectomy	39 [36.8%]	9 [12.0%]	19 [31.1%]
Time to Recurrence (months)			
Mean (±SD)	108.4 (±39.0)	53.0 (±39.9)	72.3 (±45.2)

Aim 4 was designed to test the best markers that distinguish pure from synchronous DCIS found in Aims 1 and 2 in DCIS that either did or did not recur as invasive cancer. From the results described above, we have established several key measures, mostly related to disease heterogeneity, that demonstrate significant ability to discriminate disease progression. The clinical samples shown in Table 3 above are now being used to test whether these markers can also predict disease progression. This is the key validation aspect for the study.

We have collected specimens from all cases shown in Table 3 from the 12 participating sites, identified regions of DCIS and invasive disease (from the recurrent sample when relevant and available), extracted DNA and RNA, and have slides prepared for protein analysis using Nanostring. Whole exome sequencing (WES) of the DNA, low pass whole genome sequencing of the DNA, and RNAseq on the RNA are all either complete or nearly complete. In particular, the WES data on two areas from each primary DCIS will be used to validate the genetic heterogeneity finding from Aim 1. Remaining thin sections from these cases will be used for a comprehensive Nanostring spatial analysis including our lead marker, GLUT1. These data will be used to directly validate the multivariate model developed from the data from Aim 1 and 2.

As noted above, we will have also measured a series of other parameters in the cohorts collected in Aim 4. These include global RNA expression from RNAseq (using a recently developed method called SMART3-seq), whole genome sequencing to derive copy number data, and approximately 50 protein markers on the Nanostring panels. These data sets, using technology that was not available when our DOD grant was written, will greatly increase our ability to discover markers related to disease progression which is the primary goal of this project.

What was accomplished under these goals?

Our primary goals have been met including, testing and finding evidence that genetic diversity within DCIS is associated with progression to invasive ductal carcinoma (Aim 1).
This entailed development of a bioinformatics tool for reliably detecting mutations in small amounts of fixed DNA. We also identified immunohistochemical markers that reveal intra-tumor phenotypic heterogeneity that also distinguishes pure DCIS from DCIS that is adjacent to invasive disease (Aim 2). We have acquired more radiology imaging data sets and established the computer vision algorithms for their analysis. Further, we accrued sufficient cases and controls at Duke to fulfill the Aim 1 and 2 goals of the project. Overall, we completed the proposed work in the project period along the time line that was provided.

What opportunities for training and professional development has the project provided?

We hired a new post-doctoral fellow and technical staff in the previous year to continue expanding our analysis. Luis Cisneros joined the ASU data analysis team and attended a breast cancer

meeting. Lunden Simpson joined the Duke team and has been trained in use and analysis of Nanostring. Rui Hou has been partly funded by this project for her entire PhD dissertation research, resulting in multiple conference presentations and manuscripts. Priya Narayanan has completed her PhD in the Yuan Lab.

How were the results disseminated to communities of interest?

Work based on aims 1 and 2 presented at the San Antonio Breast Cancer Symposium in December 2019, and for aim 3 at that conference in December 2017.
The work based on aim 3 resulted in several papers [2, 4, 6, 12, 13, 14]. We also presented talks and posters at SPIE Medical Imaging in February 2017, 2018, 2019, and 2020.

What do you plan to do during the next reporting period to accomplish the goals? N/A this is the final reporting period

4. IMPACT

Successful completion of this project has led to a variety of biomarkers (genetic, IHC and radiographic) to distinguish high risk from low risk DCIS. These results will be further carried forward and validated as part of the Human Tumor Atlas Consortium (HTAN).

What was the impact on the development of the principal discipline(s) of the project?

We continue to advance the field's understanding of DCIS progression and the impact of tumor heterogeneity on the fate of DCIS. The final deliverables of this proposal will impact how DCIS is regarded both by the scientific and clinical communities.

What was the impact on other disciplines?

We have contributed to emerging knowledge regarding the digital radiographic characteristics of DCIS and continue to extend the applications for machine learning in breast cancer. We are one of the most active teams in the field, as evidenced by numerous publications and invited talks.

What was the impact on technology transfer?

Nothing to report.

What was the impact on society beyond science and technology?

Nothing to report.

5. CHANGES/PROBLEMS

Changes in approach and reasons for change

There have been no changes in approach.

Actual or anticipated problems or delays and actions or plans to resolve them

None in this reporting period. Prior challenges have been reported and resolved.

Changes that had a significant impact on expenditures

None

Significant changes in use or care of human subjects, vertebrate animals, biohazards, and/or select agents

None

Significant changes in use or care of human subjects

None

Significant changes in use or care of vertebrate animals.

Not applicable.

Significant changes in use of biohazards and/or select agents

Not applicable

6. PRODUCTS

Publications

1. Grimm LJ, Neely B, Hou R, Selvakumaran V, Baker JA, Yoon SC, Ghate SV, Walsh R, Litton TP, Devalapalli A, Kim C, Soo MS, Hyslop T, **Hwang ES**, **Lo JY**. Mixed-methods study to predict upstaging of DCIS to invasive disease on mammography. AJR Am J Roentgenol. 2020 Aug 12. doi: 10.2214/AJR.20.23679. Epub ahead of print. PMID: 32783550. Published. Acknowledged federal support.

2. Hou R, Grimm LJ, Mazurowski MA, Marks JR, King L, **Maley CC**, **Hwang ES, Lo JY**, "A multitask deep learning method in simultaneously predicting occult invasive disease in ductal carcinoma in-situ and segmenting microcalcifications in mammography," Proc. SPIE. 11314, Medical Imaging 2020: Computer-Aided Diagnosis, 1131405 (23 March

2020); doi.org/10.1117/12.2549669. Published. Acknowledged federal support.

3. P Narayanan, SE Ahmed Raza, A Hall, J Marks, LKing, R West, L Hernandez, N Guppy, MDowsett, B Gusterson, **C Maley**, **S Hwang,** and Y Yuan, "Unmasking the immune microecology of ductal carcinoma in situ with deep learning" *npj Breast Cancer, in press*

4. J Hou R, Mazurowski MA, Grimm LJ, Marks JR, King LM, **Maley CC, Hwang ES**, **Lo JY**. Prediction of Upstaged Ductal Carcinoma in situ Using Forced Labeling and Domain Adaptation. IEEE Trans Biomed Eng. 2019. Epub 2019/09/11. doi: 10.1109/TBME.2019.2940195. PubMed PMID: 31502960. Published. Acknowledged federal support.

5. Grimm LJ, Miller MM, Thomas SM, Liu Y, **Lo JY, Hwang ES**, Hyslop T, Ryser MD, "Growth Dynamics of Mammographic Calcifications: Differentiating Ductal Carcinoma in Situ from Benign Breast Disease," Radiology, 182599 (2019). Epub 2019/05/22.

6. Hou R, Ren Y, Grimm LJ, Mazurowski MA, Marks JR, King L, **Maley CC, Hwang ES**, **Lo JY**, "Malignant microcalcification clusters detection using unsupervised deep autoencoders," Proc. SPIE 10950, Medical Imaging 2019: Computer-Aided Diagnosis, 109502Q (13 March 2019). Published. Acknowledged federal support.

7. Walther, V., Hiley, C.T., Shibata, D., Swanton, C., Turner, P.E., and **Maley, C.C.**: Can oncology recapitulate paleontology? Lessons from species extinctions. Nature Reviews Clinical Oncology, 12:273-285, 2015. doi:10.1038/nrclinonc.2015.12. Published. Acknowledged federal support.

8. Caulin, A.F., **Maley, C.C.:** Solutions to Peto's Paradox Revealed by Mathematical Modeling and Cross-Species Cancer Gene Analysis. Philosophical Transactions of the Royal Society of London B, 370 (1673):20140222. Published. Acknowledged federal support.

9. Aktipis, C.A., Boddy, A.M., Jansen, G., Hibner, U., Hochberg, M.E., **Maley, C.C.**, Wilkinson, G.S.: Cancer across the tree of life: Cooperation and cheating in multicellularity. Philosophical Transactions of the Royal Society of London B, 370 (1673):20140219. Published. Acknowledged federal support.

10. Noemi Andor, Trevor A. Graham, Marnix Jansen, Li C. Xia, C. Athena Aktipis, Claudia Petritsch, Hanlee P. Ji, **Carlo C. Maley**: Pan-cancer analysis of the extent and consequences of intra-tumor heterogeneity. Published. Nature Medicine 22:105-13, 2016. Acknowledged federal support.

11. **Carlo C. Maley**, Konrad Koelble, Rachael Natrajan, Athena Aktipis and Yinyin Yuan: An ecological measure of immune-cancer colocalization as a prognostic factor for breast cancer. Breast Cancer Research 17:1-13, 2015. Published. Acknowledged federal support.

12. Shi B, Grimm LJ, Mazurowski MA, Baker JA, Marks JR, King LM, Maley CC, Hwang ES, **Lo JY**, "Can Occult Invasive Disease in Ductal Carcinoma In Situ Be Predicted Using Computer-extracted Mammographic Features?" Academic Radiology, 24 (9), 1139-1147 (2017). PMC5557686. Published. Acknowledged federal support.

13. Shi B, Grimm LJ, Mazurowski MA, Baker JA, Marks JR, King LM, Maley CC, Hwang ES, **Lo JY**, Prediction of occult invasive disease in ductal carcinoma in situ using deep learning features, J Am Coll Radiol, accepted (2017). Acknowledged federal support

14. Shi B, Grimm LJ, Mazurowski MA, Marks JR, King LM, Maley CC, Hwang ES, **Lo JY**, Prediction of occult invasive disease in ductal carcinoma in situ using computer-extracted mammographic features, Proc. SPIE 10134, Medical Imaging 2017: Computer-Aided Diagnosis, Armato SG, Petrick NA, Eds., 101341I (2017). Published. Acknowledged federal support.

15. Shi B, Grimm LJ, Mazurowski MA, Marks JR, King LM, Maley CC, Hwang ES, **Lo JY**, "Can upstaging of ductal carcinoma in situ be predicted at biopsy by histologic and mammographic features?" Proc. SPIE 10134, Medical Imaging 2017: Computer-Aided Diagnosis, Armato SG, Petrick NA, Eds., 101342X (2017). Published. Acknowledged federal support.

16. Abegglen, L.M., Caulin, A.F., Chan, A., Lee, K., Robinson, R., Campbell, M.S., Kiso, W.K., Schmitt, D.L., Waddell, P.J., Bhaskara, S., Jensen, S.T., **Maley, C.C**.†, Schiffman , J. D.†: Potential Mechanisms for Cancer Resistance in Elephants and Comparative Cellular Response to DNA Damage in Humans. JAMA, 314:1850-1860, 2015. Published. Acknowledged federal support.

17. Li, X., Paulson, T.P., Galipeau, P.C., Sanchez, C.A., Liu, K., Kuhner, M.K., **Maley, C.C**., Self, S.G., Vaughan, T.L., Reid, B.J., Blount, P.L.,: Assessment of esophageal adenocarcinoma risk using somatic chromosome alterations in longitudinal samples in Barrett's esophagus. Cancer Prevention Research, 8:845-56, 2015. Published. Acknowledged federal support.

18. Kostadinov, R., **Maley, C.C**., Kuhner, M.K.: Bulk genotyping of biopsies can create spurious evidence for hetereogeneity in mutation content. PLoS Computational Biology, 12:e1004413, 2016. Published. Acknowledged federal support.

19. Andor, N., **Maley, C.C**., Ji, H. P. Genomic Instability in Cancer: Teetering on the Limit of Tolerance. Cancer Research 77:2179-2185, 2017. Published. Acknowledged federal support.

20. Tollis, M., Boddy, A. M., **Maley, C.C ,**. Peto's Paradox: How has evolution solved the problem of cancer prevention? BMC Biology 15:60, 2017. Published. Acknowledged federal support.

21. Fortunato, A., Boddy, A., Mallo, D., Aktipis, A., **Maley, C.C**. †, & Pepper, J. W. †: Natural Selection in Cancer Biology: From Molecular Snowflakes to Trait Hallmarks. Cold Spring Harbor Perspectives in Medicine, a029652, 2016. († = co-senior authors) Published. Acknowledged federal support.

22. **Maley, C.C**., Aktipis, A., Graham, T.A., Sottoriva, A., Boddy, A.M., Janiszewska, M., Silva, A.S., Gerlinger, M., Yuan, Y., Pienta, K.J., Anderson, K.S., Gatenby, R., Swanton, C., Posada, D., Wu, C.-I., Schiffman, J.D., Hwang, E.S., Polyak, K., Anderson, A.R.A., Brown, J.S., Greaves, M., Shibata, D.: Classifying the Evolutionary and Ecological Features of Neoplasms. Nature Reviews Cancer, Sept. 15, 2017. Published. Acknowledged federal support.

Citations

23. Hoon Tan, P., et al., *The 2019 WHO classification of tumours of the breast.* Histopathology, 2020.
24. Elston, C.W. and I.O. Ellis, *Pathological prognostic factors in breast cancer. I. The value of histological grade in breast cancer: experience from a large study with long-term follow-up.* Histopathology, 1991. **19**(5): p. 403-10.
25. *Consensus Conference on the classification of ductal carcinoma in situ. The Consensus Conference Committee.* Cancer, 1997. **80**(9): p. 1798-802.
26. Rimmer, A., et al., *Integrating mapping-, assembly- and haplotype-based approaches for calling variants in clinical sequencing applications.* Nat Genet, 2014. **46**(8): p. 912-918.
27. Wang, K., M. Li, and H. Hakonarson, *ANNOVAR: functional annotation of genetic variants from high-throughput sequencing data.* Nucleic Acids Res, 2010. **38**(16): p. e164

Technologies or techniques

Nothing to report

Inventions, patent applications, and/or licenses

Nothing to report

Other Products

none

Grant Funding Resulting from Extension of these results

RFA-CA-17-035 Pre-Cancer Atlas (PCA) Research Centers (U2C) (PI: Hwang; coPIs West, Maley) NCI Human Tumor Atlas Network (HTAN) 2018/09/01-2024/08/30

PCORI 1505-30497 (Hwang) Comparison of Operative versus Medical Endocrine Therapy for low risk DCIS: The COMET Trial. 2016/07/01-2023/06

BCRF 19-074 (Hwang) 2019/10/02-2020/09/30**:** Molecular and Radiologic Predictors of Invasion in a DCIS Active Surveillance Cohort.

7. PARTICIPANTS & OTHER COLLABORATING ORGANIZATIONS

What individuals have worked on the project?

Co-PI: Dr. Shelley Hwang (M.D., M.P.H.): Duke University (no change)
Co-PI: Dr. Carlo C. Maley (Ph.D.): Arizona State University (no change)

Co-Investigators:
Dr. Jeffrey Marks (Ph.D.): Duke University (no change)
Dr. Joseph Geradts (M.D.): Duke University (departed during year one)
Dr. Allison Hall (M.D.): Duke University, replacing Dr. Geradts.
Dr. Joseph Lo (Ph.D.): Duke University (no change)
Dr. Jay Baker (M.D.): Duke University (no change)
Dr. Yin Yin Yuan (Ph.D): Institute for Cancer Research, UK (no change)
Dr. Lars Grimm (M.D.): Duke University (no change)
Dr. Trevor Graham (Ph.D.): Barts Cancer Institute, Queen Mary University of London (no change)
Dr. C. Athena Aktipis (Ph.D.): Arizona State University (no change)
Dr. Shane Jensen (Ph.D.): University of Pennsylvania (departed during year one)

Post-Docs:
Dr. Mengyu Wang (Ph.D): Duke University (departed during year one)
Dr. Violet Kovacheva (Ph.D): Institute for Cancer Research, UK (departed during year two)
Dr. Narayanan (Ph.D): Institute for Cancer Research, UK, replacing Dr. Kovacheva.
Dr. Sobhani (Ph.D): Institute for Cancer Research, UK.
Dr. Lorraine King (Ph.D): Duke University (no change)
Dr. Bibo Shi (Ph.D): Duke University (departed during year two)
Dr. Rui Hou, ECE (Ph.D): student, Duke University (no change)
Tushar Fakrul Islam, Associate in Research, Duke University
Dr. Yinhao Ren, BME Ph.D. student, Duke University (no change)
Dr. Angelo Fortunato (Ph.D): Arizona State University (no change)
Dr. Diego Mallo (Ph.D): Arizona State University (no change)

Dr. Luis Cisneros (Ph.D): Arizona State University